The version of record Bastian Zinnhardt, Michael Müther, Wolfgang Roll, Philipp Backhaus, Astrid Jeibmann, Claudia Foray, Cristina Barca, Christian Döring, Bertrand Tavitian, Frédéric Dollé, Matthias Weckesser, Alexandra Winkeler, Sven Hermann, Stefan Wagner, Heinz Wiendl, Walter Stummer, Andreas H Jacobs, Michael Schäfers, Oliver M Grauer, TSPO imaging-guided characterization of the immunosuppressive myeloid tumor microenvironment in patients with malignant glioma, *Neuro-Oncology*, , noaa023, is available online at: https://doi.org/10.1093/neuonc/noaa023.

Title: TSPO imaging-guided characterization of the immunosuppressive myeloid tumor microenvironment in patients with malignant glioma

Running title: Imaging GAMs in the glioma microenvironment

Bastian Zinnhardt*†[1,2,3,4], Michael Müther†[5], Wolfgang Roll†[2], Philipp Backhaus[1,2], Astrid Jeibmann[6], Claudia Foray[1,4], Cristina Barca[1,4], Christian Döring[1], Bertrand Tavitian[7], Frédéric Dollé[8], Matthias Weckesser[2], Alexandra Winkeler[8], Sven Hermann[1,3], Stefan Wagner[2], Heinz Wiendl[9], Walter Stummer[5], Andreas H. Jacobs[1,3,4,10], Michael Schäfers‡[1,2,3], Oliver M. Grauer‡[3,9]

† *Authors contributed equally to the work;* ‡ *Authors share senior authorship*

[1] European Institute for Molecular Imaging (EIMI), University of Münster, Münster, Germany.

[2] Department of Nuclear Medicine, University Hospital Münster, Münster, Germany.

[3] Immune Image – IMI consortium.

[4] PET Imaging in Drug Design and Development (PET3D).

[5] Department of Neurosurgery, University Hospital Münster, Münster, Germany.

[6] Institute of Neuroanatomy, University Hospital Münster, Münster, Germany.

[7] Inserm UMR970, Paris Cardiovascular Research Center, Paris, France.

[8] UMR 1023, IMIV, Service Hospitalier Frédéric Joliot, CEA, Inserm, Université Paris Sud, CNRS, Université Paris-Saclay, Orsay, France.

[9] Department of Neurology with Institute of Translational Neurology, University Hospital Münster, Münster, Germany.

[10] Department of Geriatrics, Johanniter Hospital, Bonn, Germany.

*To whom correspondence should be addressed:
Bastian Zinnhardt, PhD, MBA
European Institute for Molecular Imaging (EIMI) &
Department of Nuclear Medicine, University Hospital Münster
Westfälische Wilhelms University Münster
Waldeyerstraße 15
48149 Münster, Germany
Phone: +492518349300 Fax: +492518349312
Email: zinnhardt@uni-muenster.de

Funding: This work was partly funded by the EU 7th Framework Programme (FP7/2007-2013) under grant agreement n° 278850 (INMiND), the Horizon 2020 Programme under grant agreement n° 675417 (PET3D), the 'Cells-in-Motion' Cluster of Excellence (DFG EXC1003 - CiM), the IMI2-JU under grant agreement n° 831514 (Immune-Image) and the Interdisciplinary Center for Clinical Research (IZKF core unit PIX), Münster, Germany. WR is funded by a clinician scientist rotational grant of the Medical Faculty of the University of Münster. PB is funded by a clinician scientist rotational grant of the German Research Foundation (DFG: Fa474/5, SFB1009-Z02).

Authorship: B.Z, M.M, W.R., W.S., A.H.J., M.S., O.M.G Conception, Study design, Acquisition, analysis, and interpretation of data, drafting and critical revision of the article, and final approval of the version to be published. P.B., A.J., C.D, C.F., C.B, M.W., S.W., S.H. Acquisition, analysis, and interpretation of data, drafting and critical revision of the article, and final approval of the version to be published. B.T., F.D., A.W., H.W. Analysis and interpretation of data, critical revision of the article, and final approval of the version to be published.

Conflict of interest: The authors report no competing interests.

Word count: 6243

Abstract

Background: Tumor-associated microglia and macrophages (TAMs) and myeloid-derived suppressor cells (MDSCs) are potent immunosuppressors in the glioma tumor microenvironment (TME). Their infiltration is associated with tumor grade, progression and therapy resistance. Specific tools for image-guided analysis of spatio-temporal changes in the immunosuppressive myeloid tumor compartments are missing. We aimed (i) to evaluate the role of [^{18}F]DPA-714 (TSPO) PET-MRI in the assessment of the immunosuppressive TME in glioma patients and (ii) to cross-correlate imaging findings with in-depth immunophenotyping.

Methods: To characterize the glioma TME, a mixed collective of nine glioma patients underwent [^{18}F]DPA-714-PET-MRI in addition to [^{18}F]FET-PET-MRI. Image-guided biopsy samples were immuno-phenotyped by multiparametric flow cytometry and immunohistochemistry. *In vitro* autoradiography was performed for image validation and assessment of tracer binding specificity.

Results: We found a strong relationship ($r = 0.84$, $p = 0.009$) between the [^{18}F]DPA-714 uptake and the number and activation level of glioma-associated myeloid cells (GAMs). TSPO expression was mainly restricted to HLA-DR$^+$ activated GAMs, particularly to tumor-infiltrating HLA-DR$^+$ MDSCs and TAMs. [^{18}F]DPA-714-positive tissue volumes exceeded [^{18}F]FET-positive volumes and showed a differential spatial distribution.

Conclusion: [^{18}F]DPA-714-PET may be used to non-invasively image the glioma-associated immunosuppressive TME *in vivo*. This imaging paradigm may also help to characterize the heterogeneity of the glioma TME with respect to the degree of myeloid cell infiltration at various disease stages. [^{18}F]DPA-714 may also facilitate the development of new image-guided therapies targeting the myeloid-derived TME.

Keywords: *TSPO, PET, glioma, imaging biomarker, tumor microenvironment, GAMs, TAMs, MDSCs, DPA-714*

Key points:

- TSPO and FET PET provide complementary information on tumor heterogeneity and extent.
- Combining these imaging biomarkers supports the characterization of the immunosuppressive TME.
- TSPO-PET correlates with the degree and activation of GAMs.

Importance of the study

Characterizing the immunosuppressive tumor microenvironment (TME) is essential to determine patients' treatment response. Disappointing clinical immunotherapy trials and the dominant role of immunosuppressive myeloid cells in therapy resistance and immune escape emphasize the need for novel tools investigating the TME.

We show that (i) TSPO-PET and amino acid PET provide complementary information on tumor heterogeneity and extent, (ii) the combination of both imaging biomarkers complements the non-invasive characterization of the immunosuppressive TME in a mixed collective of glioma patients, and (iii) the uptake of [^{18}F]DPA-714 in TSPO-PET strongly correlates with the extent and activation level of glioma-associated myeloid cells (GAMs).

TSPO-PET may act as a novel personalized medicine tool to determine the degree of immunosuppressive myeloid cell infiltration and thus may represent a promising prognostic imaging biomarker for mechanisms of drug sensitivity and resistance, as well as patient selection and stratification for therapeutic modulation of the immunosuppressive TME.

Introduction

Malignant gliomas are the most common primary brain tumors in adults. Intracranial neoplasms constitute the 2nd most common cause of death from intracranial disease. Current standard management consists of surgery, radio-therapy and chemotherapy with alkylating agents [1,2].

Immunotherapies are currently being actively investigated in patients with glioma. However, despite promising results in other tumor entities, clinical trials on immunotherapy have not yet shown positive results. Extensive spatial and temporal heterogeneity of the pro-tumorigenic glioma immune microenvironment (TME) represents an important obstacle for delivery of efficient (immuno-) therapies. Within the TME different glioma-associated myeloid cells (GAMs) are increased, including myeloid-derived suppressor cells (MDSCs), tumor associated macrophages (TAMs) and brain-resident microglia cells (MGs) [3–5]. In view of the importance of the immunosuppressive TME and associated challenges to develop, deliver and validate efficient therapies, improved imaging strategies targeting dynamic cellular changes in the of immunosuppressive myeloid glioma TME are urgently needed.

The current clinical imaging paradigm for gliomas consists of MRI and amino acid PET [6] facilitating tumor volume definition and metabolic activity, both aspects being important for planning of surgical resections. Furthermore, amino acid PET provides valuable additional information on proliferative activity, disease prognosis and helps with response assessment (for review: [7,8]). However, amino acid PET imaging does not provide information on the cellular composition of the glioma TME.

In contrast, targeting the 18-kDa translocator protein (TSPO) by the novel tracer [^{18}F]DPA-714 has been shown (i) to be a suitable marker for immune cell and tumor imaging in preclinical glioma models [9–12], (ii) to provide complementary information to the commonly used amino acid PET tracer [^{18}F]FET [13,14] and (iii) to be superior to standard MR imaging methods in

visualizing glioma growth and infiltration at early disease stages [15]. These findings are further supported by other groups using different TSPO-PET and SPECT radiotracers in preclinical and clinical settings [16–18].

Increased TSPO expression in human glioma and glioma cell lines has been associated with increased malignancy, poor survival and glioma invasiveness [19,20]. *In vivo*, TSPO expression in glioma models is derived from TAMs, tumor cells, and endothelial cells [13,21]. However, the exact link between glioma-associated myeloid cell infiltration, TSPO expression and radiotracer binding in different glioma entities remains to be elucidated.

To investigate the glioma TME, we performed multi-tracer PET-MRI with the second generation TSPO-PET radio tracer [^{18}F]DPA-714 in combination with [^{18}F]FET. To determine cellular sources of PET signals and tracer specificity, in-depth immunophenotyping of the glioma immune microenvironment of stereotactic biopsies was performed using flow cytometry, immunohistochemistry and *in vitro* autoradiography, including *in vitro* blocking studies.

We hypothesized that [^{18}F]DPA-714 is a translational imaging biomarker to characterize the glioma-associated myeloid-derived immunosuppressive TME *in vivo*. A combination with the commonly used amino acid tracer [^{18}F]FET and MR imaging parameters should advance our understanding of the dynamic changes and biological activity in the glioma immune microenvironment *in vivo*.

Material and Methods

Patients:

During May 2018 and 2019, additional imaging with TSPO was offered to all patients with suspicion of either primary or recurrent glioma undergoing surgical resection at our brain tumor center. Besides routine preoperative imaging, including contrast enhanced (CE) MRI and [^{18}F]FET-PET-MRI (Siemens Biograph mMR, 3 Tesla), [^{18}F]DPA-714 (TSPO) PET-MRI was performed in the frame of a compassionate use. All patients provided written informed consent on the examination and the genotyping of the Ala147Thr-polymorphism to characterize individual TSPO affinities and to exclude low affinity binders. Flow cytometric analysis analysis of biosamples and retrospective analysis of imaging data, biopsy material and clinical information were conducted following approval of the institutional ethics committee (file numbers 2010-461-f-S, 2019-276-f-S and 2019-509-f-S) and with the principles of the 1964 Declaration of Helsinki and its later amendments.

Radiochemistry

[^{18}F]FET was prepared fully-automatically in a cassette-based GE TRACERlab MX module following a synthetic two-step approach described by Pauleit *et al.* [22].

The preparation of [^{18}F]DPA-714 was performed as published by Kuhnast *et al.* [23]. For blocking studies, the concentration of [$^{18/19}$F]DPA-714 in the product solution was determined via analytical HPLC and then an appropriate amount of non-radioactive [^{19}F]DPA-714 was added to adjust a concentration increased by a factor 1000.

PET-MR imaging

PET-MR imaging was performed on a Biograph mMR system (Siemens Healthineers, Erlangen, Germany) with a 3T wide -bore MRI scanner. PET-CT imaging (patient #6) was performed on a hybrid PET–computed tomography device (mCT, Siemens, Erlangen, Germany). Image processing and reconstruction were performed with software as supplied by

the manufacturer, included homogeneous attenuation correction of the head. Patients were injected intravenously with 246.4 ± 51.6 MBq [^{18}F]FET and 247.3 ± 27.3 MBq [^{18}F]DPA-714, respectively. Dynamic PET scanning for 40 ([^{18}F]FET) or 60 minutes ([^{18}F]DPA-714) [24] was initiated with the injection of the tracer. PET images were co-registered to simultaneously acquired routine non-CE MRI images (FLAIR, T_2).

PET data analysis

Static PET images ([^{18}F]FET 20-40 min p.i.; [^{18}F]DPA-714 30-60 min p.i.) were analyzed by two nuclear medicine specialists and two neuro-radiologists blinded for clinical information and reported in consensus using the in-house developed software package MEDgical. Lesion-to-contrast-ratios were calculated for both tracers by comparing SUVmax or SUVmean in a volume-of-interest (VOI, defined by thresholding) placed over the pathological uptake pattern to the SUVmean of a control crescent-shaped region of interest (ROI) in the contralateral centrum semiovale [25].

The biologic tumor volume (BTV) of [^{18}F]FET was determined by multiplying the standardized uptake value (SUV) of the control ROI with the factor of 1.8 [25]. A similar approach was used for [^{18}F]DPA-714 thresholding. Based on our previous experience in preclinical human glioma models, [^{18}F]DPA-714 VOIs were thresholded by multiplying the standard deviation of the control ROI with a factor of three. The result was added to the mean SUV of the control ROI and used as lower threshold of the tumor uptake [13]. All patients with tracer uptake below the chosen threshold and consequently without thresholded VOI were reported with uptake ratios of one. The percentage of overlap between both radiotracers was identified by dividing the overlapping volume (ml) by the total tracer volume (ml), defined as the union of both tracer volumes. [^{18}F]DPA-714 and [^{18}F]FET exclusive areas were calculated by subtracting the overlapping volume from the respective total tracer volume. Percentages of exclusive tracer

areas were calculated by dividing the exclusive tracer volume (ml) by the total tracer volume (ml).

TSPO genotyping

The procedures for TSPO genotyping are detailed in the supplementary material and methods.

Stereotactic biopsies

Following preoperative PET and MR imaging, all patients underwent microsurgical resection applying state of the art techniques for maximal safe resections: intraoperative 5-ALA derived fluorescence, neuronavigation and intraoperative neuro-monitoring including awake craniotomies. Before starting resection after craniotomy, sampling from areas of interest as defined from preoperative imaging (CE-MRI, [^{18}F]FET and [^{18}F]DPA-PET) was performed if area of interest was deemed safe for biopsy. To allow for maximal accuracy, sampling was achieved by techniques of frameless stereotaxis including preoperative target definition (Brainlab Cranial 3.0, Brainlab AG, Munich, Germany). Sampling targets were hotspots of [^{18}F]FET tracer uptake according to current practice management guidelines [25] (Suppl. table 1). Patient #3 without hotspot was biopsied according to CE on MRI. Tissue samples were immediately stored on ice and underwent further processing on the same day.

Autoradiography

Autoradiography was performed on tumor biopsies from seven patients (Table 1). Further experimental details are found in the supplementary material and methods.

Histology, immunohistochemistry and immunofluorescence

All tumor biopsies underwent routine histopathological and molecular analyses at the Institute of Neuropathology, University Münster, Germany. Tumors were classified in accordance with

the WHO 2016 classification update of brain tumors [26]. Detailed protocols and the computer-based quantification are described in the supplementary materials and methods.

Multiparametric flow cytometry (FACS)

Tumor biopsies were extensively washed to discard blood and suction fluid. Tumor cell suspensions were isolated as previously described [27,28] and immediately stained with a panel of directly labeled monoclonal antibodies (mAbs), as specified in the supplementary Material & Methods section. To determine the frequency and phenotype of GMAs, cell debris was excluded by forward (FSC) and side scatter (SSC). $CD45^+$ leukocytes were selected in a forward scatter channel (FSC) vs CD45 plot. $CD45^+$ cells were displayed in a sideward scatter channel (SSC) vs CD11b plot to identify $CD11b^{high}$ myeloid cells. $CD11b^+$ myeloid cell subsets were defined by CD45 and CD14 expression as previously described: $CD45^{dim}CD14^+$ brain-resident MGs, tumor-infiltrating $CD45^{med}CD14^{+++}$ MDSCs and $CD45^{high}CD14^{++}$ TAMs [3,4]. Additional tumor material from a new diagnosed glioblastoma patient (IDH1-wildtype, unmethylated MGMT, 79 years old, female) was used to discriminate brain-resident MGs from tumor-infiltrating MDSCs and TAMs by CD49d expression. ([29–31]. $CD14^{++/+++}$/$HLA\text{-}DR^+$ myeloid cells were gated and analyzed for the expression of TSPO and PD-L1 (CD274).

Statistics

Statistical analyses and data visualization were performed with GraphPad Prism 7 (GraphPad Software, San Diego, CA, USA). Differences between radiotracer uptake volumes and exclusive tracer uptake were tested with a paired t-test. Uptake ratios were tested with a repeated measures one-way ANOVA with Greenhouse-Geisser correction. Multiple comparisons were performed with Tukey correction and multiplicity adjusted p values were obtained.

Differences in CD68 and TSPO infiltration between [^{18}F]DPA-714 positive and [^{18}F]DPA-714 negative patients were analyzed with an unpaired t-test. Correlation analyses were performed

with a two-tailed Pearson correlation test, followed by linear regression analyses. Significance levels were set at $p \leq 0.05$.

Results

Patient characteristics

Nine patients (mean age 42: range 29-60 years; 4 females) were included. Tissue diagnoses obtained after surgery revealed four low-grade glioma (HGG), referring to WHO grade II tumors) and five high-grade glioma (HGG), this group consisting of two WHO III tumors and three WHO grade IV tumors. See Suppl. Table 1 for full patient characteristics including molecular integrated diagnoses and follow-up data.

Seven patients were therapy naïve. Two patients were treated for recurrent disease (# 5 and #6). Patient #6 was examined after intracavitary thermotherapy with iron oxide nanoparticles and radiotherapy (NanoTherm®, MagForce AG, Berlin, Germany) [32]. The patient cohort consisted of four high affinity binder (HAB), five medium affinity binders (MAB) and no low affinity binders (LAB). During a median follow up time of 12 months after [^{18}F]DPA-714-PET, none of the patients experienced progression, malignization or death.

Multi-tracer characterization of the glioma TME

The combination of [^{18}F]FET- and [^{18}F]DPA-714-PET delivered complementary information regarding differential spatial distribution, extent and degrees of radiotracer uptake in LGG and HGG. Both tracer uptake patterns showed partial overlap with FLAIR hyperintensities (Figure 1A-D). Six patients with positive [^{18}F]FET- and [^{18}F]DPA-714-PET were identified (FET^{+}/DPA-714^{+}; Figure 1B, D, Table 1). Patient #3 lacking [^{18}F]FET uptake did not show [^{18}F]DPA-714 uptake. Uptake of [^{18}F]DPA-714 appeared even lower than in the surrounding cerebral cortex (Figure 1C, Table 2). In LGG patients with positive FET uptake, our data suggests two subgroups. Either LGG patients showed increased [^{18}F]FET and [^{18}F]DPA-714 uptake (#1 and #8, FET^{+}/DPA-714^{+}; Figure 1A, Suppl. Fig 1) or were judged as [^{18}F]DPA-714 PET negative (#7 and #3, FET^{+}/DPA-714^{-}; Figure 1B, C). All patients with initial HGG

diagnosis were positive for both, [^{18}F]FET and [^{18}F]DPA-714 uptake (FET^{+}/DPA-714^{+}; Figure 1D). The qualitative and quantitative imaging findings are summarized in Suppl. Table 1 and 2, respectively.

Threshold-based analyses of tumor volumes were performed in five patients with positive uptake for both tracers (Figure 2A). Exclusive tracer volumes (pink: FET; green: DPA-714), as well as overlapping volumes (orange) of radiotracer uptake could be identified (Figure 2B). The mean volume of [^{18}F]FET uptake was 27.3 ± 31.5 ml, whereas the mean [^{18}F]DPA-714 volumes were 50.9 ± 41.9 ml (*p = 0.1*). (Figure 2C). The percentage of exclusive tracer uptake was 39.3 ± 35.0 % for [^{18}F]FET and 65.3 ± 28.4 for [^{18}F]DPA-714 (*p = 0.24*) (Figure 2D, E). No significant differences in uptake ratios were detected (Figure 2F).

Ex vivo characterization of [^{18}F]DPA-714 on glioma biopsy material

Next, autoradiography on glioma biopsy material was performed to confirm the uptake of [^{18}F]DPA-714 *in vivo* (Figure 3A, B). A statistically significant positive correlation between the measured activity in %ID/cc from autoradiography and *in vivo* [^{18}F]DPA-714 SUV ratio was detected (r = 0.75, CI = -0.01 to 0.96, *p=0.05*).

In two cases, the [^{18}F]DPA-714 signal could be blocked by pre-incubation with a thousand-fold excess of unlabeled compound. Unlabeled compound block lead to a reduction of [^{18}F]DPA-714 binding of 95.2% in LGG and 81.6 % in HGG, proofing specificity of the tracer binding to its target.

Immunohistochemistry for CD68 and TSPO in patients with increased [^{18}F]DPA-714 uptake revealed high levels of infiltration of CD68-positive cells and extensive TSPO immunoreactivity. In contrast, patients without increased [^{18}F]DPA-714 uptake showed only minor infiltration of CD68 positive cells, as well as TSPO immunoreactivity (Figure 4A). The comparison of the percentage area of CD68 and TSPO immunoreactivity highlighted significant

differences between [^{18}F]DPA-714^{+} and [^{18}F]DPA-714^{-} patients. Patients showing [^{18}F]DPA-714 PET signals had increased CD68 infiltration (% of CD68^{+} area: 5.07 ± 1.52 % vs. 0.42 ± 0.37 %, CI = -6.9 to -2.4, *p = 0.002*) and TSPO expression (% of TSPO^{+} area: 20.06 ± 6.1 vs. 1.19 ± 0.94 %, CI = -27.8 to -9.9, *p = 0.002*) compared to PET negative patients. Positive correlations of the percentage of CD68^{+} area (r = 0.84, CI = 0.34 to 0.97, *p = 0.009*) and percentage of TSPO^{+} area (r = 0.96, CI = 0.81 to 0.99, *p = 0.0001*) with the SUVmax/mean [^{18}F]DPA-714 uptake ratios were found (Figure 4 B,C). No significant differences between LGG and HGG for CD68 and TSPO could be detected due to heterogeneous degrees of immune cell infiltration in LGG (Figure 4D).

Characterization of the cellular sources of TSPO by immunocytochemistry

To further characterize cellular subpopulations, immunocytochemistry with co-staining of TSPO with HLA-DR, Iba-1, and GFAP was performed. TSPO was widely expressed by numerous tumor-associated activated HLA-DR and Iba-1^{+} myeloid cells in a HGG patient (#4) and to a lesser extent in a LGG patient (#8) with [^{18}F]DPA-714^{+} PET (Figure 5). Only few GFAP positive astrocytes/tumor cells expressed TSPO. LGG patients without [^{18}F]DPA-714 uptake (#3 and #7) displayed only little TSPO immunoreactivity, and consequently only single Iba-1 and GFAP positive cells co-expressed TSPO (Figure 5).

Further analysis of patient-derived biopsy material ([^{18}F]DPA-714 PET positive = fraction I vs. PET negative fraction II) in a patient with glioblastoma revealed differential binding patterns of both radiotracers *in vivo*, largely irrespective of areas of CE on MRI(Suppl. Fig. 2A) and *ex vivo* (Suppl. Fig. 2B). Accordingly, different levels of TSPO were observed in immunohistochemistry (Suppl. Fig. 2C).

Characterization of cellular sources of TSPO by multi-parametric flow cytometry

To obtain further information about the cellular source of TSPO expression in glioma patients, multiparametric flow cytometry was performed as described in the M&M section. Tumor material obtained from a newly diagnosed glioblastoma patient (IDH1-wildtype, MGMT unmethylated) was used to correlate the expression of TSPO and HLA-DR in predefined subsets of myeloid cells. As depicted in Figure 6A, the tumor showed a high influx of $CD45^{+}$ leucocytes that consisted of a large proportion of $CD11b^{+}$ GMAs, that were mainly composed by $CD45^{med}CD14^{+++}$ MDSCs and $CD45^{high}CD14^{++}$ TAMs, and by a lower percentage of $CD45^{dim}CD14^{+}$ MGs. Both MDSCs and TAMs expressed high levels of CD163, HLA-DR molecules and were also positive for CD49d, a marker that was recently used to discriminate bone-marrow/blood-derived macrophages/monocytes rom brain-resident MGs (citation, see M&M section). TSPO was strongly upregulated on $HLA\text{-}DR^{+}$ MDSCs and TAMs and showed significant co-expression of programmed-death ligand 1 (PD-L1).

Accordingly, tumor biopsies in two patients, one with a $[^{18}F]FET^{+}/[^{18}F]DPA\text{-}714^{+}$ PET (patient #9, GBM WHO IV) and one with an $[^{18}F]FET^{+}/[^{18}F]DPA^{-}714^{-}$ PET (patient #7, oligodendroglioma WHO II) were analysed for the composition of myeloid cell subsets. As shown in Figure 6B, the tumor material obtained from patient #9 contained a significant number of $CD45^{+}$ leucocytes with a major fraction of $CD11b^{+}$ GMAs, that mainly consisted of MDSCs and TAMs with high expression levels of HLA-DR and strong upregulation of TSPO. In contrast, only a low amount of CD45+ leucocyte could be isolated from the tumor obtained from patient #7 with a minor fraction of $CD11b^{+}$ GAMs that were mainly restricted to TAMs and brain-resident MGs, whereas MDSCs were almost absent (Figure 6C). TSPO upregulation was less prominent when compared to the TSPO expression levels of $HLA\text{-}DR^{+}$ GMAs found in tissue taken from patient #9.

In summary, these data confirm our observation that TSPO is strongly expressed on HLADR$^+$ GAMs and suggest that the [18F]DPA-714 PET signal is largely dependent on the degree of tumor-infiltrating HLA-DR$^+$ MDSCs and HLA-DR$^+$ TAMs.

Discussion

Up to now efficient imaging biomarkers to characterize the immunosuppressive environment of gliomas that could serve as selection criteria for clinical trials are missing[33].

In this study, we demonstrate the potential of [^{18}F]DPA-714-based TSPO-PET in the non-invasive assessment of the immunosuppressive myeloid TME in a mixed collective of glioma. The combination with the commonly used tracer [^{18}F]FET provided complementary information about the glioma microenvironment, the degree of GAM infiltration and differential spatial extent and degree of tracer uptake. *In vitro* autoradiography studies and *in vitro* blocking studies confirmed specific TSPO binding *in vivo*. The combination of TSPO-PET with immunophenotyping of biopsy specimen analyzed by flow cytometry and TSPO immunohistochemistry explained differences in tracer uptake between individual patients. Interestingly, patients with differential individual degree of TSPO-positive immunosuppressive myeloid cell infiltration were identified, suggesting a role of TSPO-PET in the identification and stratification of patients in accordance to their individual immunosuppressive myeloid cell infiltration profile.

The TME is a critical regulator of cancer progression in primary and metastatic brain malignancies [34]. In gliomas and other malignancies, TAMs and MDSCs are known as potent immune suppressors, promoting tumor proliferation, migration and are known to predict the overall survival [35]. The degree of myeloid cell infiltration is associated with poor prognosis and immunotherapy failure in cancer [33 36].

TSPO has been described as a potential marker for TAMs in preclinical and clinical glioma studies. Increased TSPO expression was mainly associated with high tumor grade and worse survival [19,20], as well as grade of tumor invasion [37].

Preclinical and clinical studies have been conducted with different TSPO PET tracers, including [^{11}C]PK11195, [^{18}F]GE-180, and [^{18}F]DPA-714 [10,14,15,17,18,38]. All studies showed increased uptake in HGG. Only one study by Su *et al.* investigated LGG patients and reported no increased uptake of the first generation TSPO ligand [^{11}C]PK11195 [38]. Likewise, we observed increased [^{18}F]DPA-714 uptake and TSPO expression in all HGG patients. However, within our LGG patients our data suggests two patient subgroups; with and without [^{18}F]DPA-714 uptake, respectively. In contrast to [^{18}F]DPA-714-negative LGG patients, [^{18}F]DPA-714-positive patients displayed extensive CD68-positive immune infiltration and TSPO immunoreactivity.

Flow cytometry- and double immunohistochemistry-based characterizations of biopsy material identified activated HLA-DR^{+} GAMs as a source of TSPO signals. Particularly, tumor-infiltrating MDSCs and TAMs served as potent sources of TSPO in [^{18}F]DPA-714 PET-positive tumors, whereas GFAP positive astrocytes contributed to TSPO expression only in cases of HGG.

Su *et al.* described TSPO predominantly in neoplastic cells and only a subset of TAMs. This discrepancy may be explained by a more detailed characterization of the glioma TME by flow cytometric analysis using a wider panel of markers. To our knowledge, the link of tumor-infiltrating MDSCs as potent sources of TSPO expression in glioma, as well as the positive correlation between TSPO expression on HLA-DR^{+} GAMs and [^{18}F]DPA-714 uptake has not been described before.

PD-L1 upregulation on tumor-infiltrating MDSCs and TAMs plays a significant role in glioma immune suppression [3,39] Our data points towards an association of PD-L1 (CD274) and TSPO expression on HLA-DR+ tumor infiltrating MDSCs and TAMs. Thus, [^{18}F]DPA-714 PET might be suitable to directly visualize the accumulation of immune suppressive myeloid cells and consequently be used as novel imaging biomarker to stratify patients according to their

individual degree of immunosuppressive myeloid cell infiltrates. As MDSC- and TAM-targeted therapies in combination with immunotherapy are showing encouraging results in preclinical glioma models [34], [^{18}F]DPA-714 may also play an important role for patient selection for these targeted immunotherapies in the future.

A combination of tracers including detailed characterization of the spatial distribution has been shown to support non-invasive tumor grading and response-assessment during and after therapy [40]. To learn about the spatial relation of [^{18}F]FET and [^{18}F]DPA-714, a dedicated volumetric analysis was performed. In accordance with the work by Jensen *et al.* and Unterrainer *et al.* using other TSPO ligands, [^{18}F]DPA-714 tracer signals were spatially diverging from [^{18}F]FET signals [16,18]. A trend towards a larger extent of [^{18}F]DPA-714 volumes, as well as exclusive [^{18}F]DPA-714 volumes was observed, suggesting that both tracers provide differential biological information. Nevertheless, observed differences did not reach statistical significance, likely due to the heterogeneous and small patient population.

The role of TSPO-PET as early marker for myeloid cell infiltration, malignant transformation, and potential therapy resistance suggests potential implications for image-guided surgery based on CE-MRI, [^{18}F]FET and [^{18}F]DPA-714-PET. However, a dedicated biopsy-guided study for the estimation of ideal threshold for quantifying [^{18}F]DPA-714-volumes needs to be performed.

Non-specific uptake of the radiotracer may represent a confounding factor for the quantification of [^{18}F]DPA-714. While [^{18}F]DPA-714 specificity was successfully confirmed in several preclinical [41] and non-human primate models [42] of neurological diseases and preclinical glioma models [14], no blocking or dedicated biopsy-guided studies were performed in humans. However, Unterrainer *et al.* showed that TSPO-positive volumes exceed CE on MRI, supporting the additional value of TSPO-PET in glioma, which we were able to corroborate. Within our patient cohort the CE-MRI volumes were also exceeded by [^{18}F]DPA-714 volumes. To further underline specificity of the [^{18}F]DPA-714 signal, we provide *in vitro* autoradiograms

and TSPO histology correlated with the degree of [^{18}F]DPA-714 uptake. We here present *in vitro* blocking studies of human material for the first time, which proofed the TSPO specificity of the tracer signal.

In conclusion, a novel preoperative imaging protocol, including CE MRI, [^{18}F]FET- and [^{18}F]DPA-714- PET-MRI may allow to comprehensively characterize glioma extent and the heterogeneity of the immune tumor microenvironment in LGG and HGG. The degree of [^{18}F]DPA-714 uptake mainly reflects the influx of activated HLA-DR^{+} GAMs in the TME and may be utilized for glioma therapy planning and monitoring.

Limitations

This study is limited by the restrictions of a compassionate use approach including limited patient numbers and heterogeneity of the cohort. Larger-scale clinical trials in predetermined patient cohorts are warranted to confirm these findings. A long-term follow-up of these patients is pending to confirm the prognostic value of TSPO-PET in these patients.

Acknowledgement:

The authors thank F. Tüttelmann and A. Röpke, Institute of Human Genetics, University Hospital Münster, Münster, Germany for the analyses of TSPO binding affinities.

The authors further thank I. Hoppe, C. Möllmann, K. Thiede, A. Rothaus, and A. Kanzog for the excellent technical support for this work.

Supplementary Materials

Suppl. Fig. 1: Imaging findings of patients not shown in Figures 1-6.

Suppl. Fig. 2: Multi-modal characterization of glioma-associated tissues in glioblastoma.

Suppl. Table 1: Overview of patient characteristics.

Suppl. Table 2: Overview of radio tracer uptake ratios in thresholded volumes of interest.

Suppl. Material and Methods

References

1. Stupp R, Hegi ME, Mason WP, et al. Effects of radiotherapy with concomitant and adjuvant temozolomide versus radiotherapy alone on survival in glioblastoma in a randomised phase III study: 5-year analysis of the EORTC-NCIC trial. *Lancet Oncol*. 2009;10(5):459-466. doi:10.1016/S1470-2045(09)70025-7

2. Herrlinger U, Tzaridis T, Mack F, et al. Lomustine-temozolomide combination therapy versus standard temozolomide therapy in patients with newly diagnosed glioblastoma with methylated MGMT promoter (CeTeG/NOA-09): a randomised, open-label, phase 3 trial. *Lancet (London, England)*. 2019;393(10172):678-688. doi:10.1016/S0140-6736(18)31791-4

3. Dubinski D, Wölfer J, Hasselblatt M, et al. CD4 $^{+}$ T effector memory cell dysfunction is associated with the accumulation of granulocytic myeloid-derived suppressor cells in glioblastoma patients. *Neuro Oncol*. 2016;18(6):807-818. doi:10.1093/neuonc/nov280

4. Gabrusiewicz K, Rodriguez B, Wei J, et al. Glioblastoma-infiltrated innate immune cells resemble M0 macrophage phenotype. *JCI Insight*. 2016;1(2). doi:10.1172/jci.insight.85841

5. Gielen PR, Schulte BM, Kers-Rebel ED, et al. Elevated levels of polymorphonuclear myeloid-derived suppressor cells in patients with glioblastoma highly express S100A8/9 and arginase and suppress T cell function. *Neuro Oncol*. 2016;18(9):1253-1264. doi:10.1093/neuonc/now034

6. Albert NL, Weller M, Suchorska B, et al. Response Assessment in Neuro-Oncology working group and European Association for Neuro-Oncology recommendations for the clinical use of PET imaging in gliomas. *Neuro Oncol*. 2016;18(9):1199-1208. doi:10.1093/neuonc/now058

7. Suchorska B, Albert NL, Tonn J-C. Role of amino-tracer PET for decision-making in neuro-oncology. *Curr Opin Neurol*. 2018;31(6):720-726. doi:10.1097/WCO.0000000000000616

8. Müther M, Koch R, Weckesser M, Sporns P, Schwindt W, Stummer W. 5-Aminolevulinic Acid Fluorescence Guided-Resection of 18F-FET-PET Positive Tumor Beyond Gadolinium Enhancing Tumor Improves Survival in Glioblastoma. *Neurosurgery*. June 2019. doi:10.1093/neuros/nyz199

9. Zinnhardt B, Wiesmann M, Honold L, et al. In vivo imaging biomarkers of neuroinflammation in the development and assessment of stroke therapies - towards clinical translation. *Theranostics*. 2018;8(10). doi:10.7150/thno.24128

10. Wiesmann M, Zinnhardt B, Reinhardt D, et al. A specific dietary intervention to restore brain structure and function after ischemic stroke. *Theranostics*. 2017;7(72):493-512. doi:10.7150/thno.17559

11. Zinnhardt B, Belloy M, Fricke IB, et al. Molecular Imaging of Immune Cell Dynamics During De- and Remyelination in the Cuprizone Model of Multiple Sclerosis by [18F]DPA-714 PET and MRI. *Theranostics*. 2019;9(6). http://www.thno.org. Accessed February 18, 2019.

12. Zinnhardt B, Viel T, Wachsmuth L, et al. Multimodal imaging reveals temporal and spatial microglia and matrix metalloproteinase activity after experimental stroke. *J Cereb Blood Flow Metab*. 2015;35(11):1711-1721. doi:10.1038/jcbfm.2015.149

13. Zinnhardt B, Pigeon H, Thézé B, et al. Combined PET Imaging of the Inflammatory Tumor Microenvironment Identifies Margins of Unique Radiotracer Uptake. *Cancer Res*. 2017;77(8). doi:10.1158/0008-5472.CAN-16-2628

14. Winkeler A, Boisgard R, Awde AR, et al. The translocator protein ligand [^{18}F]DPA-714 images glioma and activated microglia in vivo. *Eur J Nucl Med Mol Imaging*. 2012;39(5):811-823. doi:10.1007/s00259-011-2041-4

15. Pigeon H, Pérès EA, Truillet C, et al. TSPO-PET and diffusion-weighted MRI for imaging a mouse model of infiltrative human glioma. *Neuro Oncol*. February 2019. doi:10.1093/neuonc/noz029

16. Jensen P, Feng L, Law I, et al. TSPO Imaging in Glioblastoma Multiforme: A Direct Comparison Between 123I-CLINDE SPECT, 18F-FET PET, and Gadolinium-Enhanced MR Imaging. *J Nucl Med*. 2015;56(9):1386-1390. doi:10.2967/jnumed.115.158998

17. Albert NL, Unterrainer M, Fleischmann DF, et al. TSPO PET for glioma imaging using the novel ligand 18F-GE-180: first results in patients with glioblastoma. *Eur J Nucl Med Mol Imaging*. 2017;44(13):2230-2238. doi:10.1007/s00259-017-3799-9

18. Unterrainer M, Fleischmann DF, Diekmann C, et al. Comparison of 18F-GE-180 and dynamic 18F-FET PET in high grade glioma: a double-tracer pilot study. *Eur J Nucl Med Mol Imaging*. 2019;46(3):580-590. doi:10.1007/s00259-018-4166-1

19. Vlodavsky E, Soustiel JF. Immunohistochemical expression of peripheral benzodiazepine receptors in human astrocytomas and its correlation with grade of malignancy, proliferation, apoptosis and survival. *J Neurooncol*. 2006;81(1):1-7. doi:10.1007/s11060-006-9199-9

20. Miettinen H, Kononen J, Haapasalo H, et al. Expression of peripheral-type benzodiazepine receptor and diazepam binding inhibitor in human astrocytomas: relationship to cell proliferation. *Cancer Res*. 1995;55(12):2691-2695. http://www.ncbi.nlm.nih.gov/pubmed/7780986. Accessed February 8, 2019.

21. Awde AR, Boisgard R, Thézé B, et al. The translocator protein radioligand 18F-DPA-714 monitors antitumor effect of erufosine in a rat 9L intracranial glioma model. *J Nucl Med*. 2013;54(12):2125-2131. doi:10.2967/jnumed.112.118794

22. Pauleit D, Stoffels G, Schaden W, et al. PET with O-(2-18F-Fluoroethyl)-L-Tyrosine in peripheral tumors: first clinical results. *J Nucl Med*. 2005;46(3):411-416. http://www.ncbi.nlm.nih.gov/pubmed/15750152. Accessed September 15, 2014.

23. Kuhnast B, Damont A, Hinnen F, et al. [18F]DPA-714, [18F]PBR111 and [18F]FEDAA1106—Selective radioligands for imaging TSPO 18kDa with PET: Automated radiosynthesis on a TRACERLAb FX-FN synthesizer and quality controls. *Appl Radiat Isot*. 2012;70(3):489-497. doi:10.1016/j.apradiso.2011.10.015

24. Lavisse S, Garcia-Lorenzo D, Peyronneau M-A, et al. Optimized Quantification of Translocator Protein Radioligand 18F-DPA-714 Uptake in the Brain of Genotyped Healthy Volunteers. *J Nucl Med*. 2015;56(7):1048-1054. doi:10.2967/jnumed.115.156083

25. Law I, Albert NL, Arbizu J, et al. Joint EANM/EANO/RANO practice guidelines/SNMMI procedure standards for imaging of gliomas using PET with radiolabelled amino acids and [18F]FDG: version 1.0. *Eur J Nucl Med Mol Imaging*.

2019;46(3):540-557. doi:10.1007/s00259-018-4207-9

26. Louis DN, Perry A, Reifenberger G, et al. The 2016 World Health Organization Classification of Tumors of the Central Nervous System: a summary. *Acta Neuropathol*. 2016;131(6):803-820. doi:10.1007/s00401-016-1545-1

27. Grauer OM, Nierkens S, Bennink E, et al. CD4+FoxP3+ regulatory T cells gradually accumulate in gliomas during tumor growth and efficiently suppress antiglioma immune responses in vivo. *Int J cancer*. 2007;121(1):95-105. doi:10.1002/ijc.22607

28. Jacobs JFM, Idema AJ, Bol KF, et al. Regulatory T cells and the PD-L1/PD-1 pathway mediate immune suppression in malignant human brain tumors. *Neuro Oncol*. 2009;11(4):394-402. doi:10.1215/15228517-2008-104

29. Zong CC. Single-cell RNA-seq study determines the ontogeny of macrophages in glioblastomas. *Genome Biol*. 2017;18(1). doi:10.1186/s13059-017-1375-z

30. Müller S, Kohanbash G, Liu SJ, et al. Single-cell profiling of human gliomas reveals macrophage ontogeny as a basis for regional differences in macrophage activation in the tumor microenvironment. *Genome Biol*. 2017;18(1). doi:10.1186/s13059-017-1362-4

31. Pinton L, Masetto E, Vettore M, et al. The immune suppressive microenvironment of human gliomas depends on the accumulation of bone marrow-derived macrophages in the center of the lesion. *J Immunother Cancer*. 2019;7(1):58. doi:10.1186/s40425-019-0536-x

32. Grauer O, Jaber M, Hess K, et al. Combined intracavitary thermotherapy with iron oxide nanoparticles and radiotherapy as local treatment modality in recurrent glioblastoma patients. *J Neurooncol*. 2019;141(1):83-94. doi:10.1007/s11060-018-03005-x

33. Kamran N, Alghamri MS, Nunez FJ, et al. Current state and future prospects of immunotherapy for glioma. *Immunotherapy*. 2018;10(4):317-339. doi:10.2217/imt-2017-0122

34. Quail DF, Joyce JA. The Microenvironmental Landscape of Brain Tumors. *Cancer Cell*. 2017;31(3):326-341. doi:10.1016/j.ccell.2017.02.009

35. Hambardzumyan D, Gutmann DH, Kettenmann H. The role of microglia and macrophages in glioma maintenance and progression. *Nat Neurosci*. 2015;19(1):20-27. doi:10.1038/nn.4185

36. Veglia F, Perego M, Gabrilovich D. Myeloid-derived suppressor cells coming of age. *Nat Immunol*. 2018;19(2):108-119. doi:10.1038/s41590-017-0022-x

37. Veenman L, Levin E, Weisinger G, et al. Peripheral-type benzodiazepine receptor density and in vitro tumorigenicity of glioma cell lines. *Biochem Pharmacol*. 2004;68(4):689-698. doi:10.1016/j.bcp.2004.05.011

38. Su Z, Roncaroli F, Durrenberger PF, et al. The 18-kDa mitochondrial translocator protein in human gliomas: an 11C-(R)PK11195 PET imaging and neuropathology study. *J Nucl Med*. 2015;56(4):512-517. doi:10.2967/jnumed.114.151621

39. Bloch O, Crane CA, Kaur R, Safaee M, Rutkowski MJ, Parsa AT. Gliomas promote immunosuppression through induction of B7-H1 expression in tumor-associated macrophages. *Clin Cancer Res*. 2013;19(12):3165-3175. doi:10.1158/1078-0432.CCR-

12-3314

40. Laukamp KR, Lindemann F, Weckesser M, et al. Multimodal imaging of patients with gliomas confirms^{11}C-MET PET as a complementary marker to MRI for noninvasive tumor grading and intraindividual follow-up after therapy. *Mol Imaging*. 2017;16. doi:10.1177/1536012116687651

41. James ML, Fulton RR, Vercoullie J, et al. DPA-714, a new translocator protein-specific ligand: synthesis, radiofluorination, and pharmacologic characterization. *J Nucl Med*. 2008;49(5):814-822. doi:10.2967/jnumed.107.046151jnumed.107.046151 [pii]

42. Lavisse S, Inoue K, Jan C, et al. [18F]DPA-714 PET imaging of translocator protein TSPO (18 kDa) in the normal and excitotoxically-lesioned nonhuman primate brain. *Eur J Nucl Med Mol Imaging*. 2015;42(3):478-494. doi:10.1007/s00259-014-2962-9

Figure legends:

Figure 1: The combination of [^{18}F]FET- with [^{18}F]DPA-714-PET reveals complementary information on glioma tissue and TME heterogeneity in LGG and HGG. In LGG two patient groups were suggested based on the degree of [^{18}F]DPA-714 uptake. All HGG patients showed increased [^{18}F]DPA-714 uptake. (A) LGG patient displaying increased [^{18}F]DPA-714 uptake in the mesial temporal lobe, whereas [^{18}F]FET remained below the threshold for the BTV in this region. (B, C) LGG patients without [^{18}F]DPA-714 uptake in the tumor regions. (D) HGG with pronounced [^{18}F]FET and [^{18}F]DPA-714 uptake. Abbreviations: LGG: low grade glioma; HGG: high grade glioma; BTV: biological-tumor-volume

Figure 2: Analysis of the spatial distribution and interrelation of radiotracer uptake. (A) Workflow from PET/MR images (top) towards determination of the tracer uptake volumes by thresholding (bottom). (B) Visualization of the spatial relation of tracer uptake. Exclusive [^{18}F]FET volumes displayed on FLAIR images in blue, centrum semiovale in yellow. Areas of tracer uptake, unique for [^{18}F]DPA-714 are displayed in purple. Overlapping tracer uptake volumes are displayed in orange. (C) Quantitative assessment of tracer uptake volumes and (D, E) percentages of exclusive radiotracer uptake volumes. (F) Comparison of tracer uptake ratios from thresholded volumes in LGG and HGG.

Figure 3: *In vitro* autoradiography of image-guided biopsy samples. (A) *In vitro* incubation with [^{18}F]DPA-714 of glioma biopsies in agreement with *in vivo* imaging and TSPO histology. (B) The percentage of incubated dose (%ID/cm²) correlates with the mean [^{18}F]DPA-714 SUV uptake ratios. (C) Incubation of a neighboring slice with a 1000-fold excess of unlabeled [^{18}F]DPA-714 leads to almost complete blocking of tracer binding. Scale bar autoradiography: 10 mm; Scale bar histopathology: 50 µm

Figure 4: Analysis and cross-correlation of biopsies with immunohistochemistry. (A) Patients with increased [^{18}F]DPA-714 uptake (#8 and #4) display increased infiltration of CD68^{+}

myeloid cells and extensive immunoreactivity for TSPO. Patients without [^{18}F]DPA-714 uptake (#7 and #3) show only minor infiltration of CD68^{+} myeloid cells and only single cells express TSPO (arrows). (B) CD68 and TSPO immunoreactivity was increased in [^{18}F]DPA-714-positive patients compared to [^{18}F]DPA-714-negative patients. (C) The area of CD68 and TSPO staining correlated with the maximum [^{18}F]DPA-714 uptake ratios. (D) No significant differences in CD68^{+} and TSPO^{+} areas could be detected when comparing LGG to HGG. Differences are likely masked by two LGG patients showing increased CD68^{+} cell infiltration and TSPO expression (pink circle). Scale bar: 100 µm

Figure 5: Molecular characterization of the cellular sources of TSPO in LGG and HGG. (A) Double immunofluorescence for TSPO with HLA-DR, Iba-1, and GFAP respectively. Patients with increased [^{18}F]DPA-714 uptake (#8 and #4) show TSPO expression in activated immune cells (HLA-DR^{+}, arrows), microglia/macrophages (Iba-1, arrows). Astrocytes (GFAP) play a minor role in cellular TSPO expression. Patients without [^{18}F]DPA-714 uptake (#7 and #3) demonstrate modest TSPO expression in single cells. Scale bar: 100 µm

Figure 6: Immunophenotpying of the myeloid cell composition by multiparametric flow cytometry (A) Representative dot plots of freshly prepared tumor material obtained from a patient with a newly diagnosed glioblastoma WHO IV. GAMs were identified as described in the M&M section. Anti-CD11b, anti-CD14 and anti-CD45 were used to distinguish CD45^{dim}CD14^{+} brain-resident MGs, CD45^{med}CD14^{+++} MDSCs and CD45^{high}CD14^{++} TAMs. Co-expression of CD163, HLA-DR and CD49d in the GAM fractions are illustrated. Histogram overlays for TSPO (green) and PD-L1(CD274) (red) expression in CD14$^{++/+++}$/HLA-DR^{+} GAMs relative to isotype control (black) are shown. (B, C) Representative dot plots with patient-specific distribution of GAMs and co-expression of HLA-DR in tumor samples obtained from a [^{18}F]FET^{+}/[^{18}F]DPA-714^{+} (patient #9) and a [18F]FET+/[^{18}F]DPA-714^{-} tumor

area (patient #7). Histogram overlays for TSPO (green) expression in $CD14^{++/+++}$/$HLA\text{-}DR^{+}$ GAMs relative to isotype control (black).

Figure 1

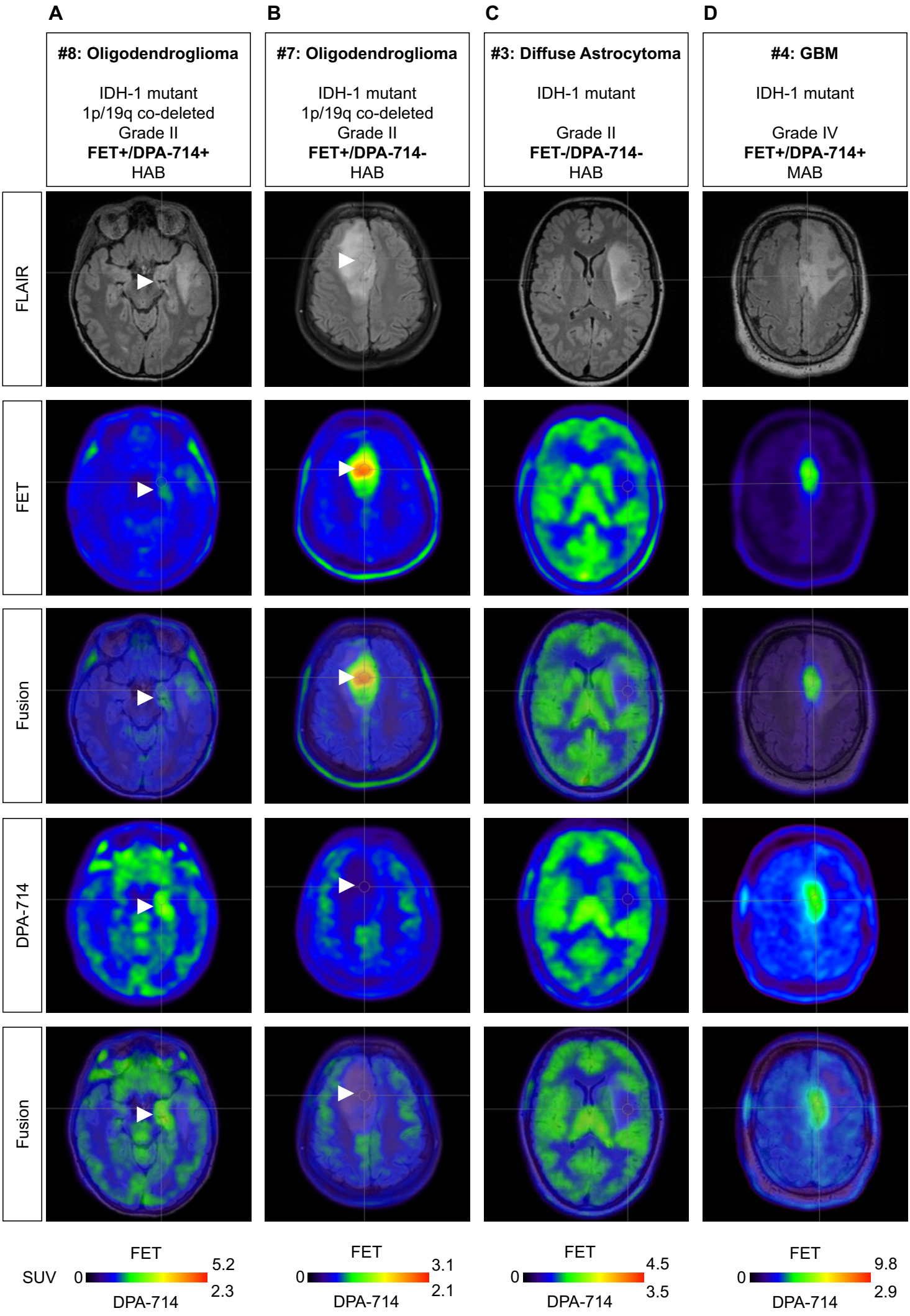
A
#8: Oligodendroglioma
IDH-1 mutant
1p/19q co-deleted
Grade II
FET+/DPA-714+
HAB
B
#7: Oligodendroglioma
IDH-1 mutant
1p/19q co-deleted
Grade II
FET+/DPA-714-
HAB
C
#3: Diffuse Astrocytoma
IDH-1 mutant
Grade II
FET-/DPA-714-
HAB
D
#4: GBM
IDH-1 mutant
Grade IV
FET+/DPA-714+
MAB
FLAIR
FET
Fusion
DPA-714
Fusion
SUV
FET
0
5.2
2.3
DPA-714
FET
0
3.1
2.1
DPA-714
FET
0
4.5
3.5
DPA-714
FET
0
9.8
2.9
DPA-714

Figure 2

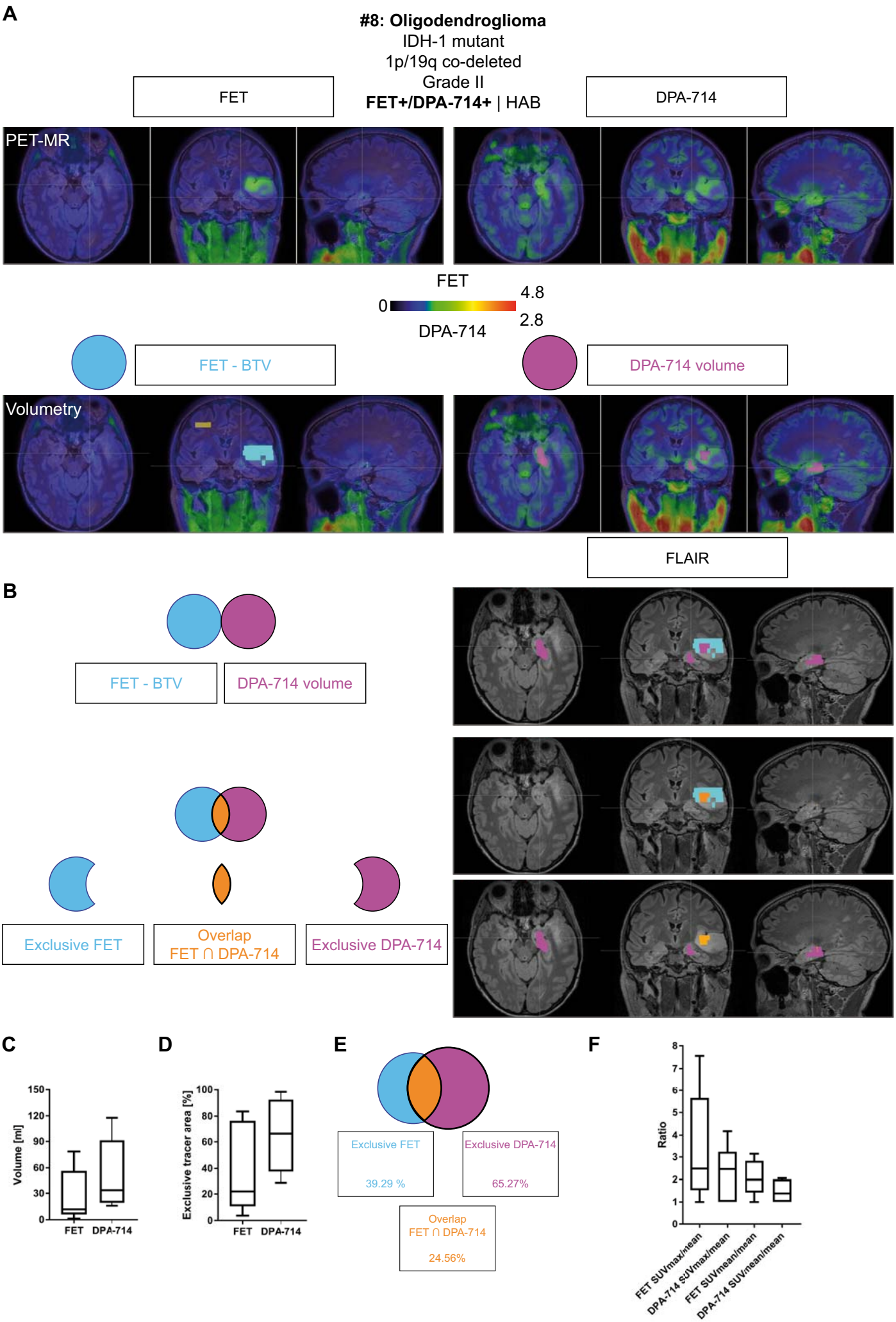
A
#8: Oligodendroglioma
IDH-1 mutant
1p/19q co-deleted
Grade II
FET+/DPA-714+ | HAB
FET
DPA-714
PET-MR
FET
4.8
0
2.8
DPA-714
FET - BTV
DPA-714 volume
Volumetry
FLAIR
B
FET - BTV
DPA-714 volume
Exclusive FET
Overlap
FET ∩ DPA-714
Exclusive DPA-714
C
Volume [ml]
150
120
90
60
30
0
FET
DPA-714
D
Exclusive tracer area [%]
100
80
60
40
20
0
FET
DPA-714
E
Exclusive FET
39.29 %
Exclusive DPA-714
65.27%
Overlap
FET ∩ DPA-714
24.56%
F
Ratio
8
7
6
5
4
3
2
1
0
FET SUVmax/mean
DPA-714 SUVmax/mean
FET SUVmean/mean
DPA-714 SUVmean/mean

Figure 3

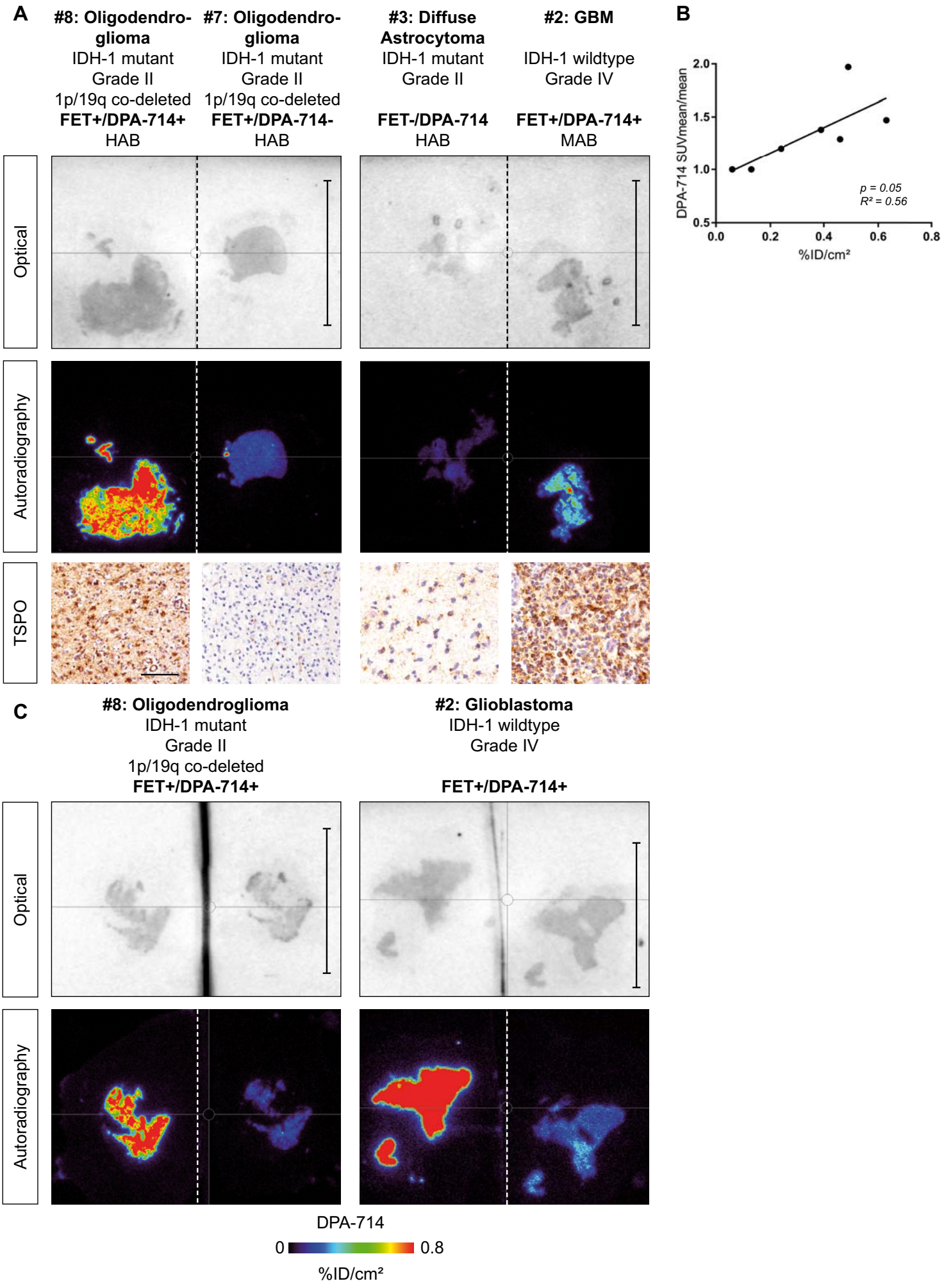
A
#8: Oligodendro-glioma
IDH-1 mutant
Grade II
1p/19q co-deleted
FET+/DPA-714+
HAB
#7: Oligodendro-glioma
IDH-1 mutant
Grade II
1p/19q co-deleted
FET+/DPA-714-
HAB
#3: Diffuse Astrocytoma
IDH-1 mutant
Grade II
FET-/DPA-714
HAB
#2: GBM
IDH-1 wildtype
Grade IV
FET+/DPA-714+
MAB
Optical
Autoradiography
TSPO
B
DPA-714 SUVmean/mean
2.0
1.5
1.0
0.5
0.0
0.2
0.4
0.6
0.8
%ID/cm²
p = 0.05
R² = 0.56
C
#8: Oligodendroglioma
IDH-1 mutant
Grade II
1p/19q co-deleted
FET+/DPA-714+
#2: Glioblastoma
IDH-1 wildtype
Grade IV
FET+/DPA-714+
Optical
Autoradiography
DPA-714
0
0.8
%ID/cm²

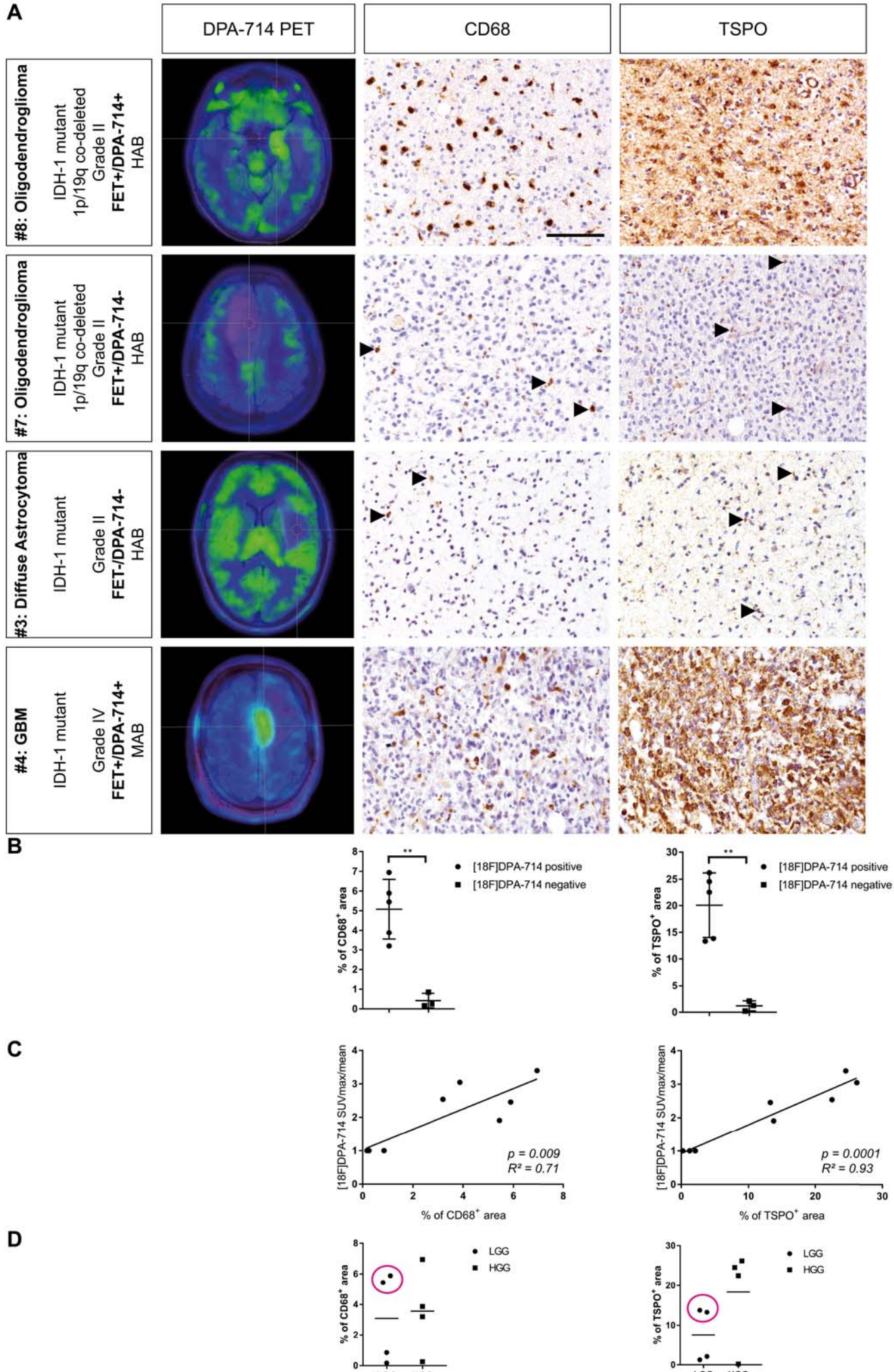
A
DPA-714 PET
CD68
TSPO
#8: Oligodendroglioma
IDH-1 mutant
1p/19q co-deleted
Grade II
FET+/DPA-714+
HAB
#7: Oligodendroglioma
IDH-1 mutant
1p/19q co-deleted
Grade II
FET+/DPA-714-
HAB
#3: Diffuse Astrocytoma
IDH-1 mutant
Grade II
FET-/DPA-714-
HAB
#4: GBM
IDH-1 mutant
Grade IV
FET+/DPA-714+
MAB
B
% of CD68+ area
[18F]DPA-714 positive
[18F]DPA-714 negative
% of TSPO+ area
C
[18F]DPA-714 SUVmax/mean
% of CD68+ area
p = 0.009
R² = 0.71
% of TSPO+ area
p = 0.0001
R² = 0.93
D
% of CD68+ area
LGG
HGG
% of TSPO+ area

Figure 5

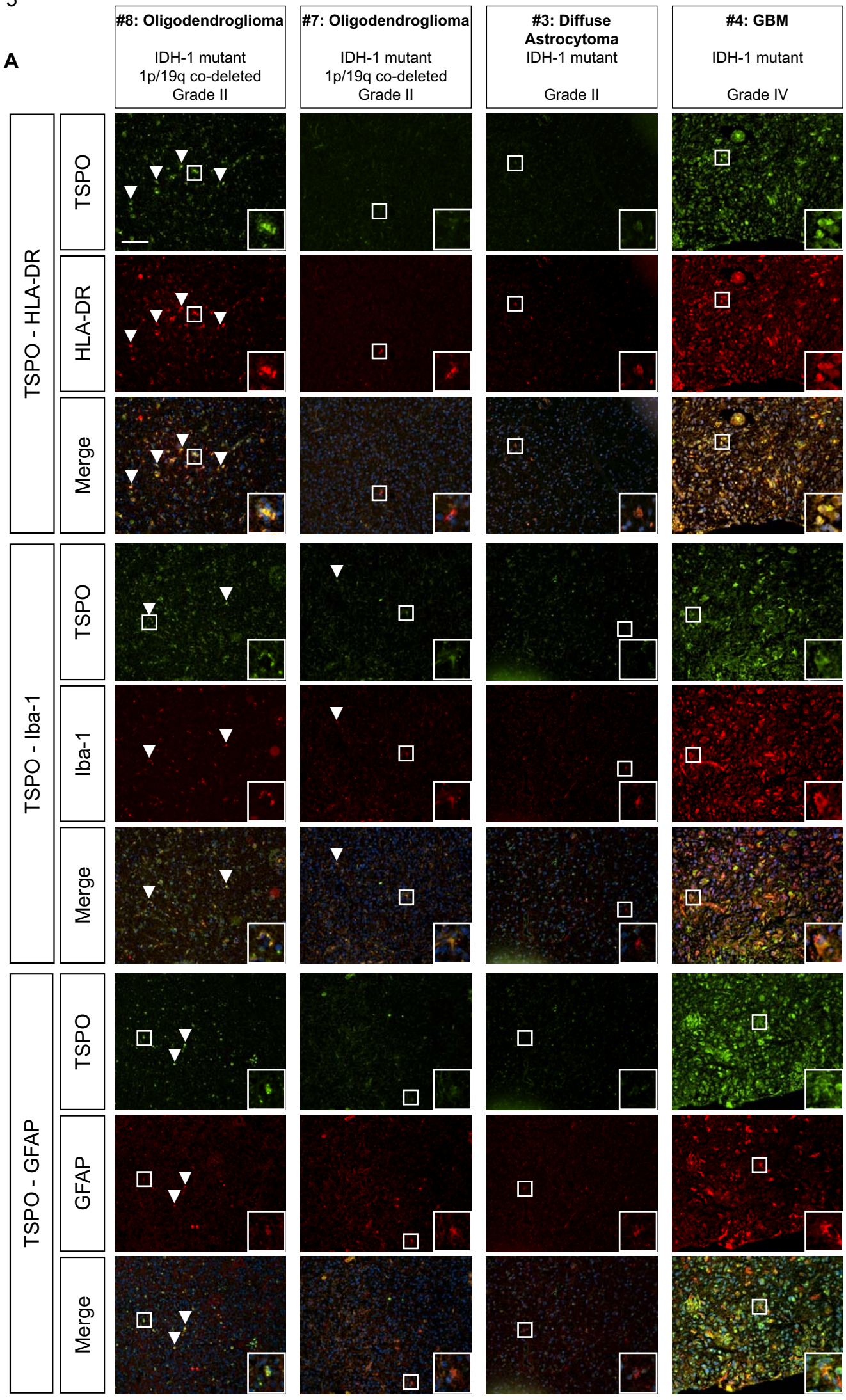
A
#8: Oligodendroglioma
IDH-1 mutant
1p/19q co-deleted
Grade II
#7: Oligodendroglioma
IDH-1 mutant
1p/19q co-deleted
Grade II
#3: Diffuse Astrocytoma
IDH-1 mutant
Grade II
#4: GBM
IDH-1 mutant
Grade IV
TSPO - HLA-DR
TSPO
HLA-DR
Merge
TSPO - Iba-1
TSPO
Iba-1
Merge
TSPO - GFAP
TSPO
GFAP
Merge

Figure 6

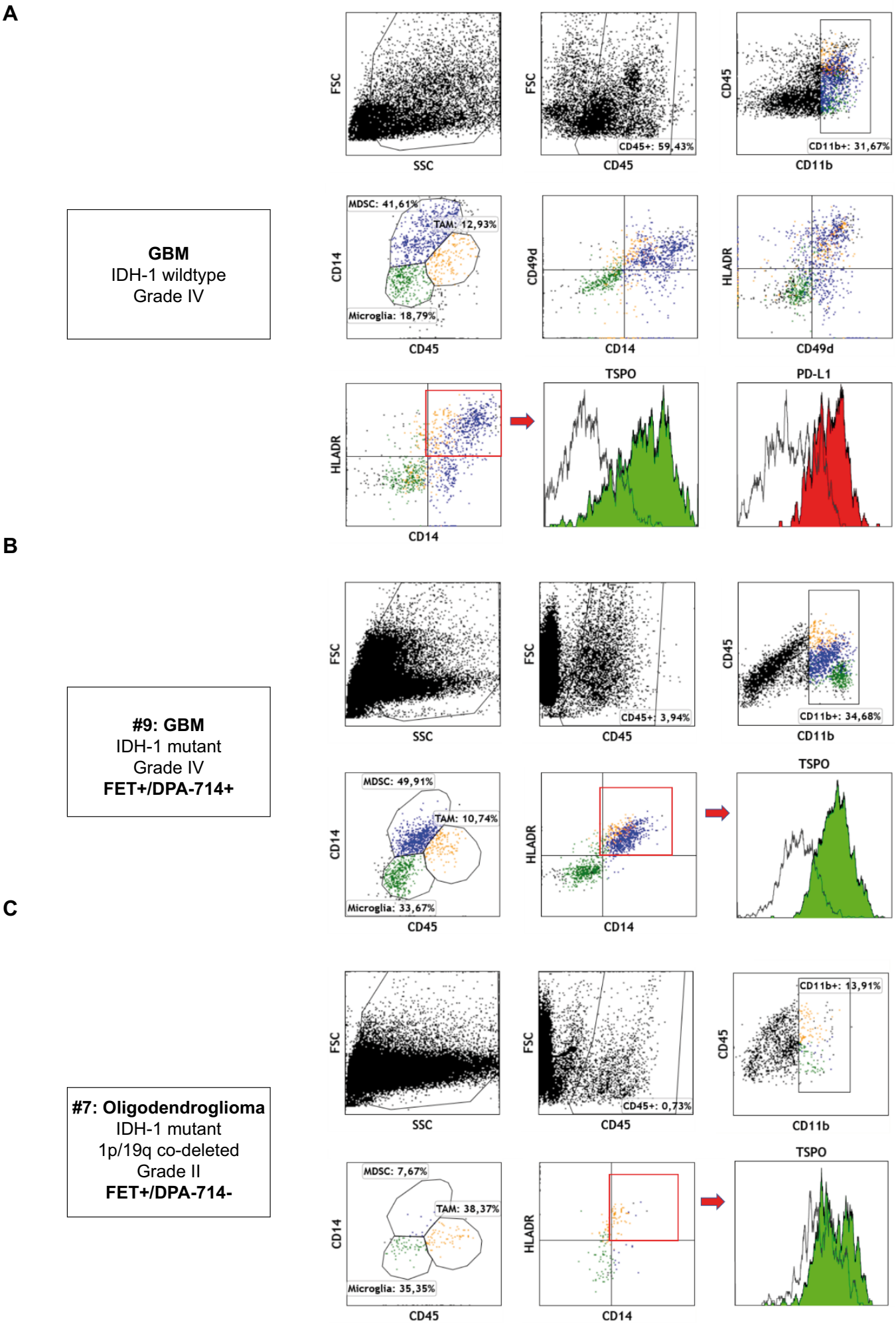
A
GBM
IDH-1 wildtype
Grade IV
FSC
SSC
CD45+: 59,43%
CD45
CD11b+: 31,67%
CD11b
MDSC: 41,61%
TAM: 12,93%
Microglia: 18,79%
CD14
CD45
CD49d
HLADR
TSPO
PD-L1
B
#9: GBM
IDH-1 mutant
Grade IV
FET+/DPA-714+
CD45+: 3,94%
CD11b+: 34,68%
MDSC: 49,91%
TAM: 10,74%
Microglia: 33,67%
C
#7: Oligodendroglioma
IDH-1 mutant
1p/19q co-deleted
Grade II
FET+/DPA-714-
CD45+: 0,73%
CD11b+: 13,91%
MDSC: 7,67%
TAM: 38,37%
Microglia: 35,35%

Suppl. Fig.1

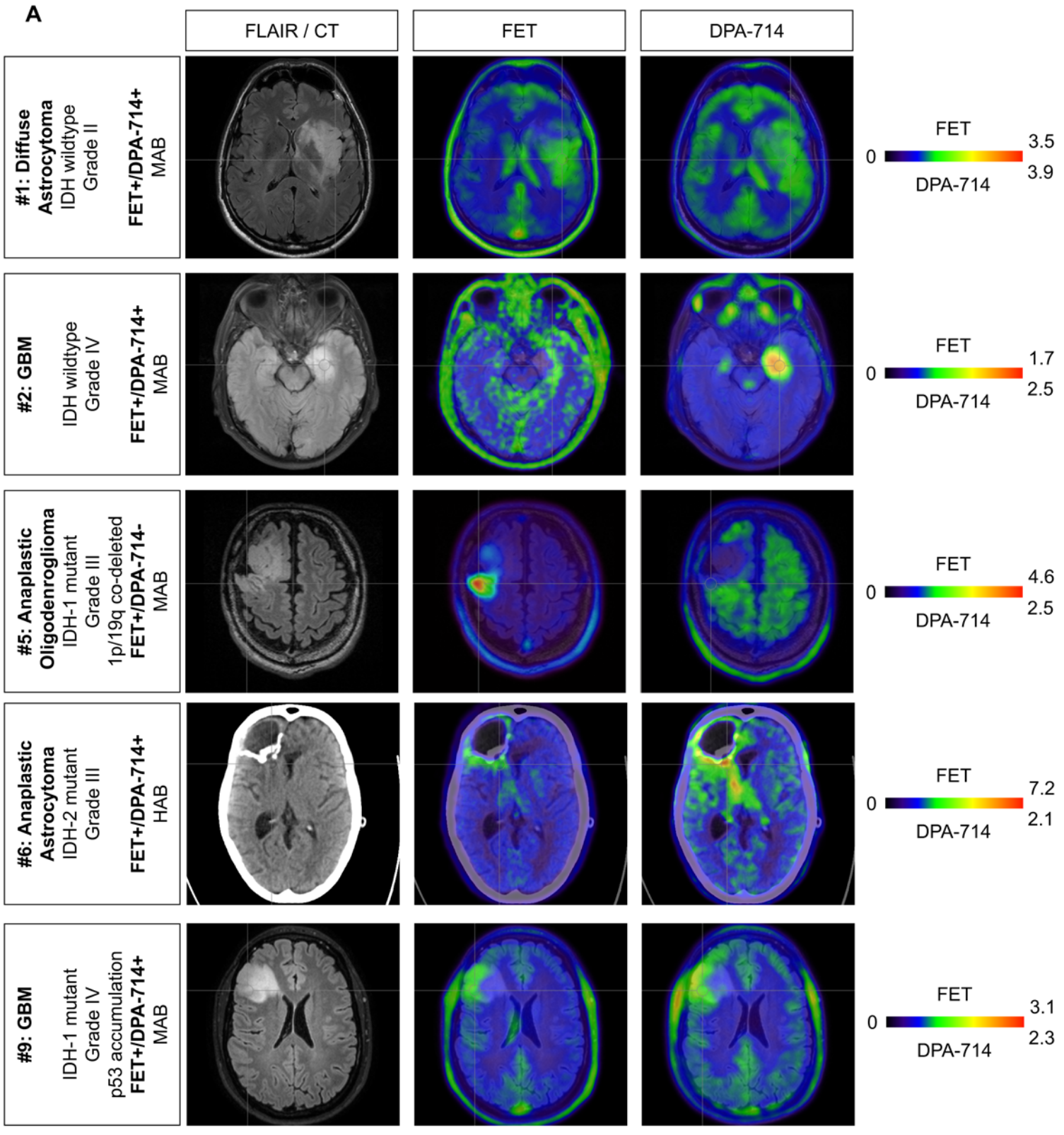
A
FLAIR / CT
FET
DPA-714
#1: Diffuse Astrocytoma
IDH wildtype
Grade II
FET+/DPA-714+
MAB
#2: GBM
IDH wildtype
Grade IV
FET+/DPA-714+
MAB
#5: Anaplastic Oligodenroglioma
IDH-1 mutant
Grade III
1p/19q co-deleted
FET+/DPA-714-
MAB
#6: Anaplastic Astrocytoma
IDH-2 mutant
Grade III
FET+/DPA-714+
HAB
#9: GBM
IDH-1 mutant
Grade IV
p53 accumulation
FET+/DPA-714+
MAB
FET
0
3.5
3.9
DPA-714
FET
0
1.7
2.5
DPA-714
FET
0
4.6
2.5
DPA-714
FET
0
7.2
2.1
DPA-714
FET
0
3.1
2.3
DPA-714

Suppl. Fig. 2

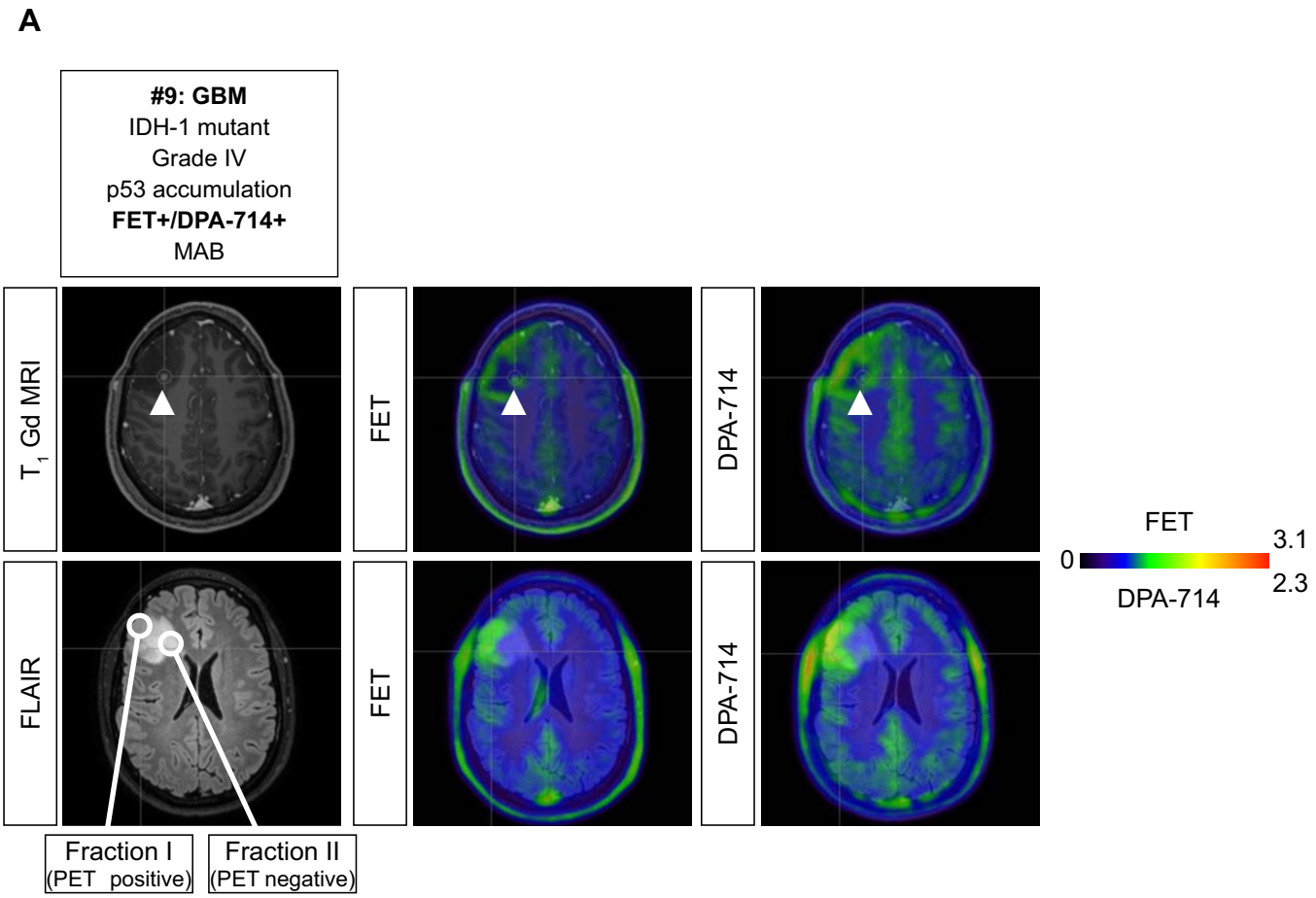
A
#9: GBM
IDH-1 mutant
Grade IV
p53 accumulation
FET+/DPA-714+
MAB
T1 Gd MRI
FLAIR
FET
FET
DPA-714
DPA-714
FET
3.1
0
2.3
DPA-714
Fraction I
(PET positive)
Fraction II
(PET negative)

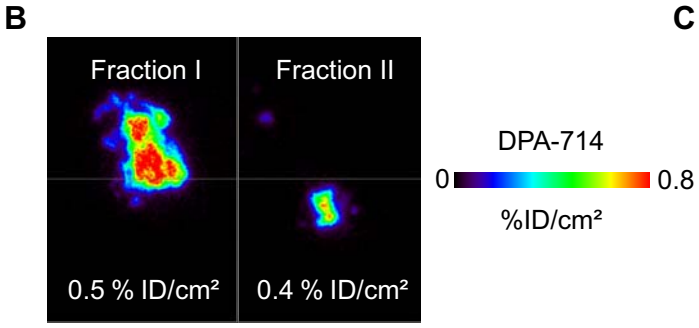
B
Fraction I
Fraction II
0.5 % ID/cm²
0.4 % ID/cm²
DPA-714
0
0.8
%ID/cm²

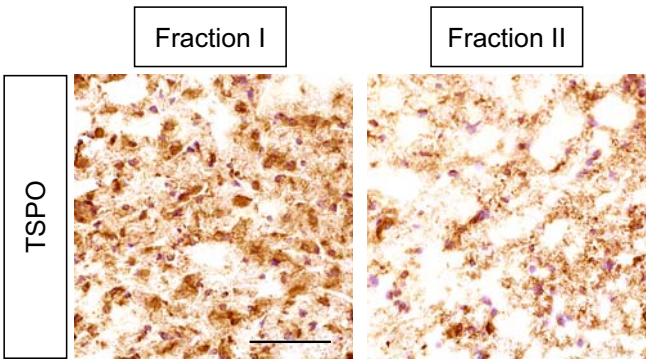
C
Fraction I
Fraction II
TSPO

Supplementary figure legends

Suppl. Fig. 1: Imaging findings of patients not shown in Figures 1-6.

Suppl. Fig. 2: Multi-modal characterization of glioma-associated tissues in glioblastoma. (A, top row). Spatial [^{18}F]FET and [^{18}F]DPA-714 uptake was largely independent from T_1 gadolinium contrast enhancement (arrows). Two image-guided biopsies were taken from a [^{18}F]DPA-714-positive (Fraction I) and [^{18}F]DPA-714-negative area (Fraction II). (B) *In vitro* autoradiography confirmed different tracer uptake between the two fractions. (C) Histological confirmation with TSPO immunohistochemistry. Scale bar autoradiography: 10 mm; Scale bar histology: 100 µm

Suppl. Table 1: Overview of patient characteristics.

#	Age	Sex	Diagnosis	Previous therapy	TSPO binding affinity*	[^{18}F]FET	[^{18}F]DPA-714	FACS	AR	Biopsy site
1	43	male	Diffuse Astrocytoma Grade II WHO (IDH wild-type, ATRX retained)	naive	MAB	+	+	N	N	FET+/DPA-714+
2	60	male	Glioblastoma Grade IV WHO (IDH wild-type, ATRX retained, MGMT methylated)	naive	MAB	+	+	N	Y	FET+/DPA-714+
3	29	female	Diffuse Astrocytoma Grade II WHO (IDH-1 mutant, ATRX loss)	naive	HAB	-	-	N	Y	CE on MRI
4	51	male	Glioblastoma Grade IV WHO (IDH-1 mutant, ATRX retained, MGMT methylated)	naive	MAB	+	+	Y	Y	FET+/DPA-714+
5	59	male	Anaplastic Oligodendroglioma Grade III WHO (IDH-1 mutant, 1p/19q co-deleted)	Two microsurgical resections with diagnosis of oligodendroglioma, IDH-mutated and 1p/19q-codeleted (Grade II WHO)	MAB	+	-	N	Y	FET+
6	32	female	Anaplastic Astrocytoma Grade III WHO (IDH-2 mutant, ATRX loss)	Two microsurgical resections, radiochemotherapy with temozolomide, cyclic temozolomide, re-irradiation, combined intracavitary thermotherapy with iron oxide nanoparticles and radiotherapy	HAB	+	+	Y	N	FET+/DPA-714+
7	35	female	Oligodendroglioma Grade II WHO (IDH-1 mutant, 1p/19q co-deleted)	naive	HAB	+	-	Y	Y	FET+
8	40	female	Oligodendroglioma Grade II WHO (IDH-1 mutant, 1p/19q co-deleted)	naive	HAB	+	+	N	Y	FET+/DPA-714+
9	31	male	Glioblastoma Grade IV WHO (IDH-1 mutant, ATRX loss)	naive	MAB	+	+	Y	Y	FET+/DPA-714+

*HAB: high affinity binder, MAB: mixed affinity binder

Suppl. Table 2: Overview of radio tracer uptake ratios in thresholded volumes of interest.

	Dose			[^{18}F]FET PET (Tumor)		[^{18}F]DPA-714 PET(Tumor)	
#	**FET (MBq)**	**DPA-714 (MBq)**	**Body weight (kg)**	**SUVmax/SUVmean**	**SUVmean/SUVmean**	**SUVmax/SUVmean**	**SUVmean/SUVmean**
1	197	231	81	2.05	1.86	2.46	2.04
2	291	267	75	n/a	n/a	3.05	1.20
3	175	193	57	1.00	1.00	1.00	1.00
4	320	250	105	6.42	3.14	2.54	1.38
5	201	260	71	7.55	3.08	1.32	1.29
6	227	275	76	2.48	1.99	4.18	2.06
7	275	275	80	4.88	2.57	1.00	1.00
8	232	253	76	3.20	2.21	1.91	1.47
9	300	222	90	2.37	1.84	3.40	1.97
Median	**232.0**	**253.0**	**76.0**	**2.8**	**2.1**	**2.5**	**1.4**
Range	**175-320**	**193-275**	**57-105**	**1-7.55**	**1-3.14**	**1-3.4**	**1-2.06**

*n/a: [^{18}F]FET not quantifiable, due to delayed acquisition.

Supplementary material and methods:

Autoradiography

Tumor biopsies were embedded in TissueTek OCT (TissueTek OCT Weckert Labortechnik, Kitzingen, Germany) and immediately snap frozen. 20 µm sections of the tumor biopsies were cut on a freezing microtome (Leica) and mounted on microscope slides. For binding assays two tumor specimens were mounted adjacent to each other on one slide. Images were acquired for 90 min in a microimager (Biospace Lab, Nesles la Vallee, France).

Slides were incubated for 20 min with 408 ± 100 kBq [^{18}F]DPA-714. After incubation, slides were washed 3 x 5 min in fresh buffer and immediately prepared for image acquisition.

For blocking experiments, two neighboring tumor slices were mounted and either incubated with comparable doses of [^{18}F]DPA-714 with a thousand-fold excess of unlabelled compound. Data were analyzed using the in-house developed software MEDgical. For analysis, an ellipsoid ROI covering the whole tumor specimen was delineated on optical images. ROIs were manually thresholded to span the tumor specimens. Obtained counts were normalized to the incubated dose (%ID) and the surface of the specimen (%ID/cm^2).

Flow cytometry

Freshly prepared cell suspensions from tumor biopsies were washed, filtered through a 70 µM cell strainer and stained with a panel of directly labeled monoclonal antibodies (mAbs). 2-5x10^5 were washed with PBS+1% FCS and incubated for 30 minutes at 4° C. The antibody mixtures included anti-CD206-PE (Phycoerythrin), anti-HLADR-ECD (Phycoerythrin-Texas Red-X), anti-CD14-PC5.5 (Phycoerythrin-Cyanine 5.5), anti-CD163- or CD49d-PE/Cy7 (Phycoerythrin-Cyanine 7), anti-CD33-APC (Allophycocyanin), anti-CD11b-APC-Alexafluor700, anti-CD16-APC-Alexafluor750, anti-CD15-PacificBlue, and anti-CD45-KromeOrange (obtained from Beckman Coulter, Krefeld, Germany, and Biolegend, Koblenz,

Germany). For TSPO staining, an Alexa488-labelled anti-PBR antibody [EPR5384], and the corresponding isotype control [EPR25A] (obtained from abcam, Cambridge, UK) were used. For PD-L1 staining, we used an anti-CD274-APC mAb and the corresponding isotype control (obtained from Biolegend, Koblenz, Germany). All samples were analyzed using the NaviosTM flow cytometer and the Kaluza 2.1 Software (Beckman Coulter, Krefeld, Germany).

TSPO Genotpying

As the binding of second generation TSPO ligands may be affected by the Ala147Thr-polymorphism and to exclude patients with low binding affinities, TSPO genotyping was performed as previously described by Genomic DNA was extracted from EDTA-preserved blood using standard techniques. PCR was performed in a volume of 20 µl with approximately 200 ng DNA and 5 pmol/µl forward primer (5'-TCAGGTGGCATGACTGTTCC-3') and reverse primer (5'-GCATGCAGAAAGCACAGGAC-3') using Biotaq DNA polymerase and dNTPs (Bioline, Luckenwalde; Germany). For sequencing, PCR products were treated with ExoSAP-IT (USB Corporation, Cleveland, OH, USA). The sequencing reaction was performed using the BigDye Terminator v3.1 Cycle Sequencing Kit (Applied Biosystems, Carlsbad, CA, USA). The data was analyzed on a 3730 DNA Analyser (Applied Biosystems).

Histology, immunohistochemistry and immunofluorescence

Adjacent 5-10 µm cryosections from autoradiography samples were post-fixed in ice cold methanol, washed in PBS and incubated over night at 4 °C using antibodies against translocator binding protein (TSPO; 1:250, rabbit anti-TSPO, NBP1-95674, AB_11015478, Novus Biologicals, Cambridge, UK), glial fibrillary protein (GFAP; 1:1000, chicken anti GFAP, ab4674, RRID:AB_304558, abcam, Cambridge, UK), ionized calcium-binding adapter molecule 1 (Iba-1; 1:250, goat anti Iba1, ab107159 AB_10972670; abcam, Cambridge, UK), and HLA-DR (1:500, mouse anti HLA-DR, ab20181, RRID:AB_445401, abcam, Cambridge, UK). After 3 x 5 min washing in PBS, slices were incubated for 60 min at room temperature

with the secondary antibodies: Alexa Fluor 488 conjugated anti-rabbit (1:800, A-21206, Life Technologies), Alexa Fluor 555 conjugated anti-goat (1:800, A-21432, Life Technologies), or DSB-X™ Biotin Goat Anti-Chicken IgG (1:800; Life Technologies). Nuclei were stained with DAPI (0.2 µg/ml, 6335.1, Carl Roth, Karlsruhe, Germany) Slides were mounted with Mowiol (0713.1, Carl Roth, Karlsruhe, Germany).

In addition to cryo sections, paraffin embedded sections (3 µm) of the tumor were obtained from the Department for Neuropathology for immunohistochemistry for CD68 (1:1000, mouse monoclonal anti-CD68, supernatant from KiM1P hybridoma cells, kindly provided by Prof. Klapper, Institute of Pathology, Kiel) and antibodies specified above. Slides were processed as described before [13,18]. All images were acquired with a combined fluorescence-light microscope (Nikon Eclipse NI-E, Nikon, Tokyo, Japan).

Immunohistochemistry of CD68 and TSPO (n=8) were quantified at a 20 fold magnification over the whole field of view using the Fiji software package. Background corrected images were color deconvoluted using the automatic “color deconvolution tool” and automatically thresholded using the “auto thresholding tool”. The percentage area of staining was estimated using the “analyze particles” tool.